Journal of Zhejiang University-SCIENCE A (Applied Physics & Engineering)
ISSN 1673-565X (Print); ISSN 1862-1775 (Online)
www.zju.edu.cn/jzus; www.springerlink.com
E-mail: jzus@zju.edu.cn

Prediction of vibrations induced by trains on line 8 of Beijing metro*

De-yun DING†1, Shashank GUPTA[2], Wei-ning LIU[1], Geert LOMBAERT[2], Geert DEGRANDE[2]

([1]*School of Civil Engineering, Beijing Jiaotong University, Beijing 100044, China*)

([2]*Department of Civil Engineering, K. U. Leuven, B3001, Heverlee, Belgium*)

†E-mail: dyding2301@163.com

Received May 22, 2009; Revision accepted July 30, 2009; Crosschecked Jan. 12, 2010

Abstract: This paper mainly discusses the problem of ground-borne vibrations due to the planned line 8 of Beijing metro which passes under the National Measurement Laboratory. A lot of vibration sensitive equipments are placed in the laboratory. It is therefore necessary to study the impact of vibrations induced by metro trains on sensitive equipments and important to propound a feasible vibration mitigation measure. Based on the coupled periodic finite element-boundary element (FE-BE) method, a 3D dynamic track-tunnel-soil interaction model for metro line 8 has been used to predict vibrations in the free field induced by trains running at variable speeds between 30 km/h and 80 km/h. Four types of track structures commonly used on the Beijing metro network have been considered: (1) high resilience direct fixation fasteners, (2) Vanguard fasteners, (3) a floating slab track and (4) a floating ladder track. For each of these track types, the vibration isolation efficiency has been compared. The results of the numerical study can be used to predict vibrations in nearby buildings and to decide upon effective vibration countermeasures.

Key words: Ground-borne vibrations, Coupled periodic finite element-boundary element (FE-BE) method, Track structure, Vibration isolation efficiency

doi:10.1631/jzus.A0900304 **Document code:** A **CLC number:** U231; U213.2

1 Introduction

With the speedy development of urban mass transit system, more and more environmental concerns are focused on the vibrations from underground trains. Vibrations can arise from the passage of trains inside the tunnel and spread through the tunnel and surrounding soil into nearby buildings. Vibrations may cause discomfort to people and interfere with sensitive equipments, such as those used in scientific research organizations, universities, hospitals and high-tech industries.

In recent years, there has been an increasing focus on the impact of vibrations induced by underground trains on sensitive equipments in buildings in the vicinity of the Beijing metro network. For instance, lines 4 and 10 respectively pass at close proximity of the Physics Laboratory of Beijing University and China Academy of Space Technology, in which a lot of sensitive equipments could be affected by the operation of metro trains (Liu W.N. *et al.*, 2005; Liu W.F. *et al.*, 2006; Gupta *et al.*, 2008). The planned lines 8 and 15 pass under the National Measurement Laboratory and Tsinghua University, respectively, where the operation of sensitive equipments might be disturbed by metro trains induced vibrations (Ding *et al.*, 2008). It is therefore very important and urgent to study the impact of vibrations induced by metro trains, if necessary, to propound a feasible vibration mitigation measure.

This paper mainly discusses the problem of vibrations due to metro trains on line 8 of Beijing metro. Based on the coupled periodic finite element-boundary element (FE-BE) method (Clouteau *et al.*, 2005; Degrande *et al.*, 2006; Gupta, 2008), a 3D dynamic track-tunnel-soil interaction model for line 8 has been used to predict the vibrations in the free field from trains running at variable speeds between 30 km/h and 80 km/h. Four types of track structures

* Project supported by the National Natural Science Foundation of China (Nos. 50538010 and 50848046), and the Research Council of K. U. Leuven (Bilateral Project BIL07/07), Belgium

commonly used on the Beijing metro network have been considered: (1) high resilience direct fixation fasteners, (2) Vanguard fasteners, (3) a floating slab track and (4) a floating ladder track. The vibration isolation efficiency of these track types has been compared. The results of the numerical study can be used to predict vibrations in nearby buildings and to implement effective vibration countermeasures.

2 Problem outline

The construction of line 8 is divided into two phases: I and II. Phase I, from South Gate of Forest Park station to Beitucheng station, also named the Olympic sub-branch, was completed on July 19, 2008 and served the Beijing 2008 Olympic Games. Phase II, currently under construction, is also separated into two sections: the north extension (from Huilongguan East station to South Gate of Forest Park station) and the south extension (from Beitucheng station to Meishuguandongjie station).

The north extension of line 8 passes at very close proximity of the National Measurement Laboratory which is located in the south of Yongtai station, as shown in Fig.1. The minimum and maximum horizontal distances from the tunnel centerline to the laboratory building are 13.7 m and 56.6 m, respectively. A lot of sensitive equipments are located in the region of 40 m far away from the tunnel centerline.

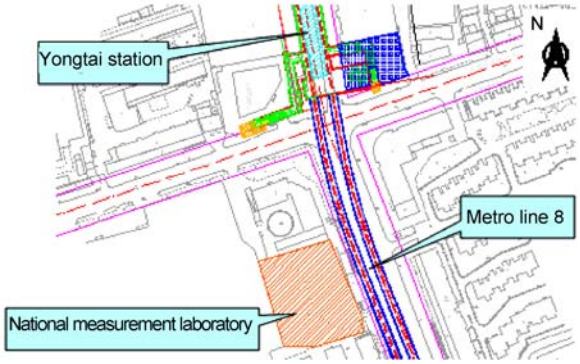

Fig. 1 Location of the National Measurement Laboratory and the Yongtai station of line 8

The future operation of line 8 is a matter of concern. Hence, it is very urgent to study the impact of metro trains induced vibrations on the operation of sensitive equipments and to propose effective vibration countermeasures.

2.1 Characteristics of the tunnel

The planned tunnels in the south of Yongtai station are two parallel shield tunnels with the precast reinforced concrete lining at 17.85 m below the free ground surface (Fig. 2). The distance between the tunnel axes is 12.1 m and each tunnel has an outer radius of 3 m and a wall thickness of 0.2 m. The tunnel lining consists of six circumferential segments connected by bolts for each ring. The reinforced concrete lining has a Young's modulus E_t=3.5×10^{10} Pa, a Poisson's ratio ν_t=0.25, a density ρ_t=2500 kg/m^3 and a hysteretic material damping ratio β_t=0.02. The tunnel invert is filled by the concrete with a Young's modulus E_i=2.85×10^{10} Pa, a Poisson's ratio ν_i=0.2, a density ρ_i=2500 kg/m^3 and a hysteretic material damping ratio β_i=0.02.

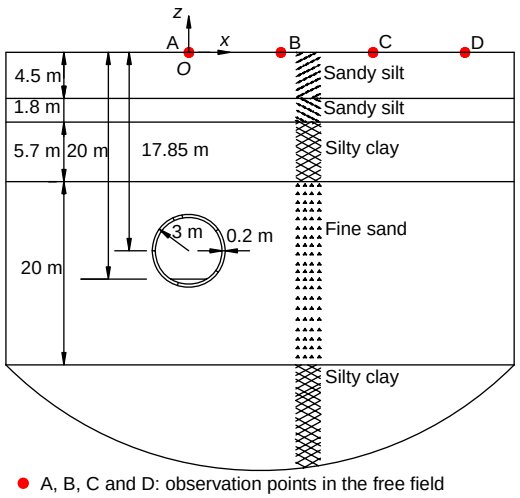

Fig. 2 Cross-section of the tunnel in the south of Yongtai station

2.2 Characteristics of the soil

The geological section map in the south of Yongtai station indicates that there are chiefly five layers of soil from top to bottom: sandy silt, sandy silt, silty clay, fine sand and silty clay (Fig. 2). The dynamic soil characteristics are summarized in Table 1.

2.3 Characteristics of the track

Fig. 3 illustrates the cross-section and plan sketch of four kinds of track structures that are commonly used on the Beijing metro network.

The DTVI$_2$ fasteners are typical of the high resilience direct fixation fasteners (DF) used on Beijing metro network. Generally, they are directly installed

on short sleepers. The rail pads with a high stiffness of 5×10^7 N/m are placed to discretely support the T-60 rails at an interval of 0.6 m. T-60 rails have a cross-sectional area of 7.725×10^{-3} m^2, a mass per unit length of 60.64 kg/m and a bending stiffness of 6.434×10^6 N·m^2.

Table 1 Dynamic soil characteristics in the south of Yongtai station of line 8

Layer No.	C_s (m/s)	C_p (m/s)	ρ (kg/m^3)	ν (-)	β (-)
1	166	319	1970	0.39	0.04
2	179	595	2000	0.45	0.04
3	256	488	2020	0.31	0.04
4	314	610	1990	0.32	0.03
5	328	665	2050	0.34	0.04

C_s is the pressure wave velocity; C_p is the shear wave velocity; ρ is the mass density; ν is the Poisson's ratio; and β is the material damping ratio

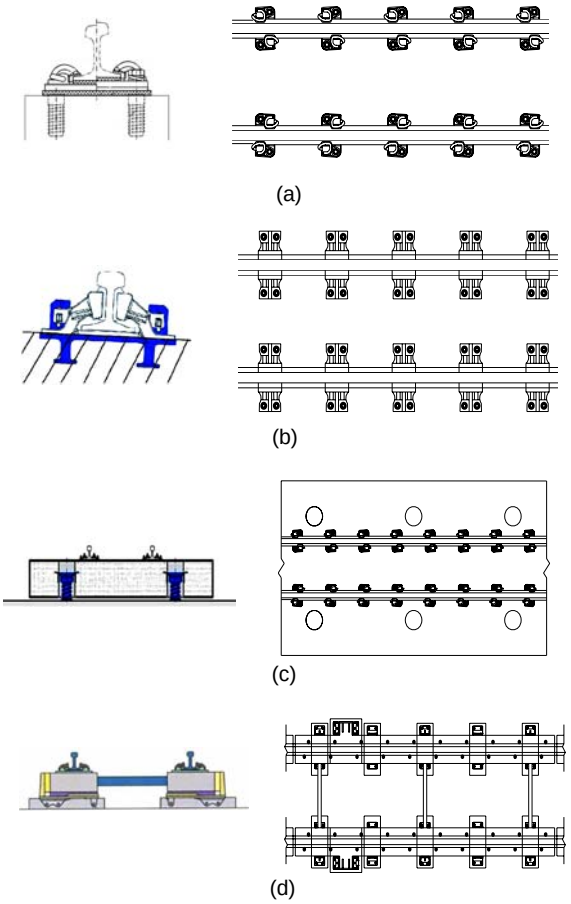

Fig. 3 Cross-section (left) and plan (right) sketch of four kinds of track structures. (a) High resilience direct fixation fasteners; (b) Vanguard fasteners; (c) Floating slab track; (d) Floating ladder track

Compared with ordinary fasteners, Vanguard fasteners (VF) have lower vertical stiffness. They can confine the torsion motion of rails. The vertical stiffness of VF is 6×10^6 N/m and the fasteners discretely support the T-60 rails at an interval of 0.6 m.

Floating slab track (FST) called mass-spring system is a typical isolation measure and has been largely applied in underground railway to mitigate vibrations (Wilson *et al*., 1983; Nelson, 1996; Lombaert *et al*., 2006; Kuo *et al*., 2008). FST could isolate vibration level up to 40 dB, and its eigenfrequency is usually less than 15 Hz (Ding *et al*., 2007).

The FST is supported by two rows of steel springs with a stiffness of 6.9×10^6 N/m and an interval of 1.8 m along the tunnel axis direction. The width and thickness of the slab are 3.5 m and 0.45 m, respectively. The slab has a density of 2500 kg/m^3. The rails and rail pads are the same to those in the DF.

Floating ladder track (FLT) is also named lightweight-spring system with a shape of ladder. Its structural concept is small-mass soft-suspended system so that it can reduce structure-borne noise with a very lightweight construction (Okuda *et al*., 2004; Hosking and Milinazzo, 2007; Xia *et al*., 2009). It mainly consists of two longitudinal prestressed sleepers, resilient bearings and steel pipes. The length, width and thickness of the sleeper are 6.15 m, 0.46 m and 0.185 m, respectively. The sleepers with a density of 2680 kg/m^3 rest on the resilient bearings with a stiffness of 2×10^7 N/m and an interval of 1.25 m along the tunnel axis direction. The steel pipes connect two sleepers and have an interval of 2.4 m along the tunnel axis direction.

2.4 Characteristics of the train

The variable voltage and variable frequency (VVVF) style rolling stock will be produced to operate on metro line 8. The train is composed of 6 carriages with each length of 19 m. The bogie distance L_b on all carriages is 12.6 m, and the axle distance L_a is 2.3 m. The total mass of the train is 3.42×10^5 kg, which results in an axle load of 1.398×10^5 N. The mass of the carriage that is full of passengers is 4.3×10^4 kg, while the mass of the bogie and axle are 3.6×10^3 kg and 1.7×10^3 kg, respectively. The primary suspension has the stiffness of 1.4×10^6 N/m and the damping of 3.0×10^4 N·s/m. The second suspension has the stiffness of 5.8×10^5 N/m and the damping of

1.6×10^5 N·s/m.

The speed of the train of the Beijing metro varies between 30 km/h and 80 km/h. These are typical values of the train speed on Beijing metro network. The speeds of 30 km/h, 45 km/h, 60 km/h and 80 km/h are considered in this study.

3 Numerical modelling of line 8

To predict metro trains induced vibrations at the National Measurement Laboratory on line 8, the dynamic track-tunnel-soil interaction system is modeled by the coupled periodic FE-BE method based on the classical domain decomposition technique, considering that a finite element method is used for the track and the tunnel and a boundary element method is used for the soil that is modeled as a horizontally layered elastic half-space (Clouteau *et al*., 2005; Degrande *et al*., 2006; Gupta, 2008).

3.1 Governing equations

The coupled periodic FE-BE method makes use of the Floquet transform to exploit the periodicity L of geometry and to restrict the problem domain Ω to a single bounded reference cell $\tilde{\Omega}$ (Degrande *et al*., 2006), as shown in Fig. 4. The problem domain Ω is decomposed into two subdomains: the tunnel Ω_t and the soil Ω_s. The boundary $\partial\tilde{\Omega}$ of the reference cell is decomposed into the free surface $\tilde{\Gamma}_{\mathrm{s}\sigma}$ of the soil and the boundaries Σ_0 and Σ_L on which periodic conditions are imposed. The reference cell $\tilde{\Omega}$ is also decomposed into the tunnel $\tilde{\Omega}_\mathrm{t}$ and the soil $\tilde{\Omega}_\mathrm{s}$. The interface between these subdomains is denoted by $\tilde{\Sigma}_{\mathrm{ts}}$. A surface force $\tilde{\boldsymbol{f}}_\mathrm{t}$ is applied on the boundary $\tilde{\Gamma}_{\mathrm{t}\sigma}$ which is the free surface of the tunnel. Using the Floquet transform, all displacement $\hat{\boldsymbol{u}}_\Delta(\boldsymbol{x},\omega)$ and traction $\hat{\boldsymbol{t}}_\Delta(\boldsymbol{x},\omega)$ fields defined on the periodic domain Ω are transformed to the fields $\tilde{\boldsymbol{u}}_\Delta(\tilde{\boldsymbol{x}},\kappa_y,\omega)$ and $\tilde{\boldsymbol{t}}_\Delta(\tilde{\boldsymbol{x}},\kappa_y,\omega)$ restricted on the reference cell $\tilde{\Omega}$. Here the subscript Δ can be s or t to denote the soil or the tunnel, respectively.

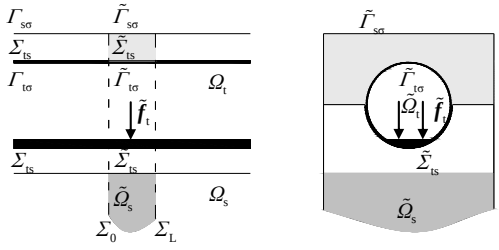

Fig. 4 Notations for periodic domains

The Navier equation in the soil domain $\tilde{\Omega}_\mathrm{s}$ and the boundary conditions on $\tilde{\Gamma}_{\mathrm{s}\sigma}$ are given as follows for every frequency $\omega\in IR$ and wavenumber $\kappa_y\in[-\pi/L, +\pi/L]$:

$$\mathrm{div}\tilde{\boldsymbol{\sigma}}_\mathrm{s}(\tilde{\boldsymbol{u}}_\mathrm{s})=-\rho_\mathrm{s}\omega^2\tilde{\boldsymbol{u}}_\mathrm{s},\ \text{in}\ \tilde{\Omega}_\mathrm{s}, \tag{1}$$

$$\tilde{\boldsymbol{t}}_\mathrm{s}(\tilde{\boldsymbol{u}}_\mathrm{s})=\boldsymbol{0},\ \text{on}\ \tilde{\Gamma}_{\mathrm{s}\sigma}, \tag{2}$$

$$\tilde{\boldsymbol{u}}_\mathrm{s}(\tilde{\boldsymbol{x}})=\exp(-\mathrm{i}\kappa_y L)\tilde{\boldsymbol{u}}_\mathrm{s}(\tilde{\boldsymbol{x}}-L\boldsymbol{e}_y),\ \text{on}\ \Sigma_\mathrm{L}, \tag{3}$$

where Eq. (3) enforces the periodicity condition of the second kind on the soil displacement vector $\tilde{\boldsymbol{u}}_\mathrm{s}(\tilde{\boldsymbol{x}})$, and $\boldsymbol{e}_y$ refers to the longitudinal unit vector.

The following Navier equations and boundary conditions hold in the tunnel domain $\tilde{\Omega}_\mathrm{t}$ with the boundary $\tilde{\Gamma}_{\mathrm{t}\sigma}$:

$$\mathrm{div}\tilde{\boldsymbol{\sigma}}_\mathrm{t}(\tilde{\boldsymbol{u}}_\mathrm{t})=-\rho_\mathrm{t}\omega^2\tilde{\boldsymbol{u}}_\mathrm{t},\ \text{in}\ \tilde{\Omega}_\mathrm{t}, \tag{4}$$

$$\tilde{\boldsymbol{t}}_\mathrm{t}(\tilde{\boldsymbol{u}}_\mathrm{t})=\tilde{\boldsymbol{f}}_\mathrm{t},\ \text{on}\ \tilde{\Gamma}_{\mathrm{t}\sigma}, \tag{5}$$

$$\tilde{\boldsymbol{u}}_\mathrm{t}(\tilde{\boldsymbol{x}})=\exp(-\mathrm{i}\kappa_y L)\tilde{\boldsymbol{u}}_\mathrm{t}(\tilde{\boldsymbol{x}}-L\boldsymbol{e}_y),\ \text{on}\ \Sigma_\mathrm{L}. \tag{6}$$

Continuity of displacements and equilibrium of stresses should hold on the tunnel-soil interface $\tilde{\Sigma}_{\mathrm{ts}}$:

$$\tilde{\boldsymbol{u}}_\mathrm{s}=\tilde{\boldsymbol{u}}_\mathrm{t},\ \text{on}\ \tilde{\Sigma}_{\mathrm{ts}}, \tag{7}$$

$$\tilde{\boldsymbol{t}}_\mathrm{s}(\tilde{\boldsymbol{u}}_\mathrm{s})+\tilde{\boldsymbol{t}}_\mathrm{t}(\tilde{\boldsymbol{u}}_\mathrm{t})=\boldsymbol{0},\ \text{on}\ \tilde{\Sigma}_{\mathrm{ts}}. \tag{8}$$

3.2 Response to moving loads

Fig. 5 shows that the vertical loads moving at a speed v along the longitudinal direction y are applied on the coupled track-tunnel-soil system. In the fixed frame of reference, the distribution of n_a vertical axle loads can be expressed by the summation of the product of Dirac functions that determine the time-dependent position $\boldsymbol{x}_m=\{x_{m0},\ y_{m0}+vt,\ z_{m0}\}^\mathrm{T}$ and the time history $g_m(t)$ of the mth axle load (Gupta *et al*., 2008):

$$\boldsymbol{f}(\boldsymbol{x},t)=\sum_{m=1}^{n_a}\delta(x-x_{m0})\delta(y-y_{m0}-vt)\delta(z-z_{m0})g_m(t)\boldsymbol{e}_z, \tag{9}$$

where y_{m0} is the initial position of the mth axle that moves at a train speed v along the y-axis, and $\boldsymbol{e}_z$ refers to the vertical unit vector.

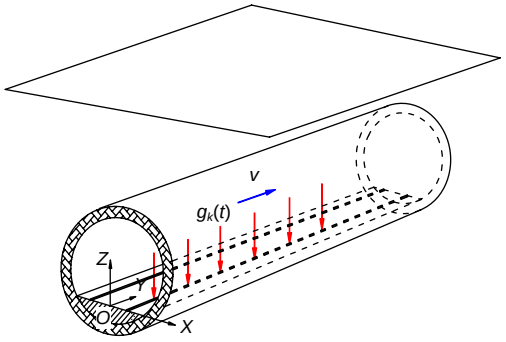

Fig. 5 Moving loads in the tunnel

Eq. (9) can be changed using a Fourier transformation from the time domain to the frequency domain as follows:

$$\hat{f}_j(\boldsymbol{x},\omega)=\frac{1}{v}\sum_{m=1}^{n_a}g_m\left(\frac{y-y_{m0}}{v}\right)\left[\exp\left(-i\frac{\omega}{v}(y-y_{m0})\right)\right] \times\delta(x-x_{m0})\delta(z-z_{m0})\delta_{zj}, \tag{10}$$

where $\rho\hat{b}_j(\boldsymbol{x},\omega)$ is the frequency domain expression of the axle load in index notation.

The response in the frequency domain $\hat{u}_i(\boldsymbol{x},\omega)$ at the receiver $\boldsymbol{x}$ due to n_a axle loads can be written as the superposition of the load distribution along y-axis (Gupta *et al.*, 2008):

$$\hat{u}_i(\boldsymbol{x},\omega)=\int_{-\infty}^{+\infty}\hat{f}_j(\boldsymbol{x}',\omega)\hat{h}_{ji}(\boldsymbol{x}',\boldsymbol{x},\omega)\mathrm{d}\boldsymbol{x}', \tag{11}$$

where $\hat{h}_{ji}(\boldsymbol{x}',\boldsymbol{x},\omega)$ is the transfer function, denoting the displacement at $\boldsymbol{x}$ in the $\boldsymbol{e}_i$ direction, which is due to a unit load applied at $\boldsymbol{x}'$ in the $\boldsymbol{e}_j$ direction.

To substitute Eq. (10) into Eq. (11), and then to elaborate the dependency of the transfer function $\hat{h}_{ji}(\boldsymbol{x}',\boldsymbol{x},\omega)$ on the source coordinates. The response $\hat{u}_i(\boldsymbol{x},\omega)$ can be given as

$$\hat{u}_i(x,y,z,\omega)=\frac{1}{v}\sum_{m=1}^{n_a}\int_{-\infty}^{+\infty}g_m\left(\frac{y'-y_{m0}}{v}\right) \times\exp\left[-i\frac{\omega}{v}(y'-y_{m0})\right] \times\hat{h}_{zi}(x_{m0},y',z_{m0},x,y,z,\omega)\mathrm{d}y'. \tag{12}$$

Introducing a charge of variable according to $\tau=(y'-y_{k0})/v$, Eq. (12) becomes

$$\hat{u}_i(x,y,z,\omega)=\sum_{m=1}^{n_a}\int_{-\infty}^{+\infty}g_m(\tau)\exp(-i\omega\tau) \times\hat{h}_{zi}(x_{m0},y_{m0}+v\tau,z_{m0},x,y,z,\omega)\mathrm{d}\tau. \tag{13}$$

Based on the Floquet transform method, an infinite periodic structure can be analyzed by confining the problem domain Ω to a single periodic reference cell $\tilde{\Omega}$. If the spatial period is L, the position $\boldsymbol{x}$ of any point in the problem domain is decomposed as $\boldsymbol{x}=\tilde{\boldsymbol{x}}+nL\boldsymbol{e}_y$, where $\tilde{\boldsymbol{x}}$ is the position in the reference cell and n is the cell number. The response due to moving loads in case of periodic domains can be obtained (Chebli *et al.*, 2006):

$$\hat{u}_i(\tilde{y}+nL,\omega)=\frac{1}{2\pi}\sum_{m=1}^{n_a}\int_{-\infty}^{+\infty}\hat{g}_m(\tilde{\omega})\int_{-L/2}^{L/2}\exp(-\mathrm{i}k_y\tilde{y}') \times\tilde{h}_{zi}(\tilde{y}',\tilde{y},\kappa_y,\omega)\mathrm{d}\tilde{y}'\exp[-\mathrm{i}k_y(nL-y_{m0})]\mathrm{d}k_y, \tag{14}$$

where $\kappa_y=k_y-2m\pi/L$ and $k_y=(\omega-\tilde{\omega})/v$. The transfer function in the frequency-wavenumber domain $\tilde{h}_{zi}(\tilde{y}',\tilde{y},\kappa_y,\omega)$ is the Floquet transform of the transfer function in the frequency-spatial domain $\hat{h}_{zi}(\tilde{y}',\tilde{y}+nL,\omega)$.

From Eq. (14) it can be seen that once the transfer function $\tilde{h}_{zi}(\tilde{y}',\tilde{y},\kappa_y,\omega)$ and the frequency content of the axle load $\hat{g}_m(\tilde{\omega})$ are known, the response due to moving loads can be calculated.

3.3 Transfer functions

When the reference cell of the tunnel is restricted, the displacement field $\tilde{\boldsymbol{u}}_t(\tilde{\boldsymbol{x}},\kappa_y,\omega)$ in the tunnel is decomposed on the basis of the functions $\tilde{\psi}_p(\tilde{\boldsymbol{x}},\kappa_y)$

(Clouteau *et al*., 2005; Degrande *et al*., 2006):

$$\tilde{\boldsymbol{u}}_{\mathrm{t}}(\tilde{\boldsymbol{x}},\kappa_y,\omega)=\sum_{p=1}^{M}\tilde{\psi}_{\mathrm{p}}(\tilde{\boldsymbol{x}},\kappa_y)\alpha_{\mathrm{p}}(\kappa_y,\omega), \tag{15}$$

where $\tilde{\psi}_{\mathrm{p}}(\tilde{\boldsymbol{x}},\kappa_y)$ is the kinematical basis that complies with the periodicity condition of the second kind and $\alpha_{\mathrm{p}}(\kappa_y,\omega)$ is the modal coordinate.

The soil displacement $\tilde{\boldsymbol{u}}_{\mathrm{s}}(\tilde{\boldsymbol{x}},\kappa_y,\omega)$ can be expressed as the superposition of waves radiated through the tunnel into the soil (Clouteau *et al*., 2005; Degrande *et al*., 2006):

$$\begin{aligned}\tilde{\boldsymbol{u}}_{\mathrm{s}}(\tilde{\boldsymbol{x}},\kappa_y,\omega)&=\tilde{\boldsymbol{u}}_{\mathrm{sc}}(\tilde{\boldsymbol{u}}_{\mathrm{t}})(\tilde{\boldsymbol{x}},\kappa_y,\omega)\\&=\sum_{p=1}^{M}\tilde{\boldsymbol{u}}_{\mathrm{sc}}(\tilde{\psi}_{\mathrm{p}})(\tilde{\boldsymbol{x}},\kappa_y,\omega)\alpha_{\mathrm{p}}(\kappa_y,\omega),\end{aligned} \tag{16}$$

where the displacement field $\tilde{\boldsymbol{u}}_{\mathrm{sc}}(\tilde{\boldsymbol{u}}_{\mathrm{t}})$ corresponds to the displacement field radiated in the soil due to the tunnel motion $\tilde{\boldsymbol{u}}_{\mathrm{t}}$ on the interface $\tilde{\Sigma}_{\mathrm{ts}}$.

The weak or variational formulation of the problem results in a dynamic tunnel-soil interation equation in the frequency-wavenumber domain (Clouteau *et al*., 2000; 2005; Degrande *et al*., 2006):

$$\begin{aligned}&[\boldsymbol{K}_{\mathrm{t}}(\kappa_y)-\omega^2\boldsymbol{M}_{\mathrm{t}}(\kappa_y)+\boldsymbol{K}_{\mathrm{s}}(\kappa_y,\omega)]\boldsymbol{\alpha}(\kappa_y,\omega)\\&\quad=\boldsymbol{F}_{\mathrm{t}}(\kappa_y,\omega),\end{aligned} \tag{17}$$

where $\boldsymbol{K}_{\mathrm{t}}(\kappa_y)$ is the dynamic stiffness matrix of the tunnel, $\boldsymbol{M}_{\mathrm{t}}(\kappa_y)$ is the mass matrix of the tunnel, $\boldsymbol{K}_{\mathrm{s}}(\kappa_y,\omega)$ is the dynamic stiffness matrix of the soil, $\boldsymbol{\alpha}(\kappa_y,\omega)$ is the matrix of the modal coordinates, and $\boldsymbol{F}_{\mathrm{t}}(\kappa_y,\omega)$ is the external force matrix.

One tunnel in the south of Yongtai station is modeled as a periodic structure with spatial period L =0.6 m. The reference cell of the tunnel is modeled by 8-node solid elements (Fig. 6a). The rails, sleepers and steel pipes are modeled using Euler-Bernoulli beam elements. The slab is modeled by plate elements, considering that it is continuous along the tunnel axis direction. The rail pads and the slab (or sleeper) bearings are represented using spring elements. All of four tracks are considered as periodic structures with a periodicity L=0.6 m (Figs. 6b–6d). Each of four types of track structures is efficiently incorporated in the tunnel using the Bampton-Craig substructuring technique (Bampton and Craig, 1968) which can describe the kinematics of the track-tunnel system as a superposition of the track modes on a rigid base and the quasi-static transmission of the free tunnel modes into the track (Degrande *et al*., 2006; Gupta, 2008).

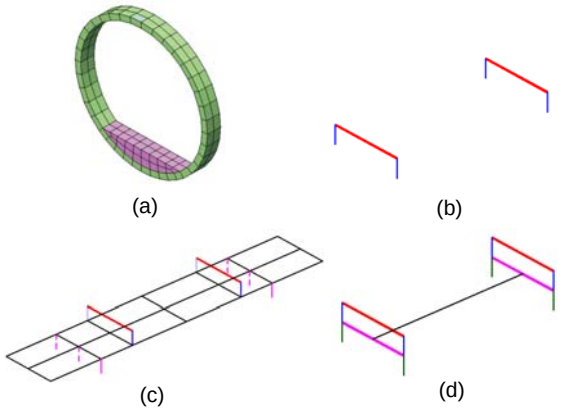

Fig. 6 Finite element model of the reference cell. (a) Tunnel; (b) DF and VF; (c) FST; (d) FLT

The kinematical basis for the free tunnel consisting of M=60 modes has been used at each wavenumber, and for four types of track structures, the kinematical basis includes 8 (DF), 8 (VF), 10 (FST) and 10 (FLT) modes on a rigid base, respectively. Fig. 7 shows the first in-plane free tunnel mode at 14.7 Hz, the first out-of-plane free tunnel mode at 111.4 Hz and the first track modes at zero wavenumber on a rigid base for DF at 186.4 Hz, VF at 64.6 Hz, FST at 7 Hz and FLT at 35.5 Hz, respectively.

From Eqs. (15)–(17), the displacement field in the reference cell of the tunnel-soil system can be obtained in the frequency-wavenumber domain. As the track is incorporated in the tunnel by the Bampton-Craig substructuring technique, the displacement field of the track-tunnel-soil system in the frequency domain at any point $\boldsymbol{x}$ is acquired after calculation of the inverse Floquet transform.

The observation points in the free field, where the response is predicted, are marked in Fig. 2. The coordinates of these observation points A, B, C and D are respectively (0 m, 0 m, 0 m), (20 m, 0 m, 0 m), (40 m, 0 m, 0 m) and (60 m, 0 m, 0 m).

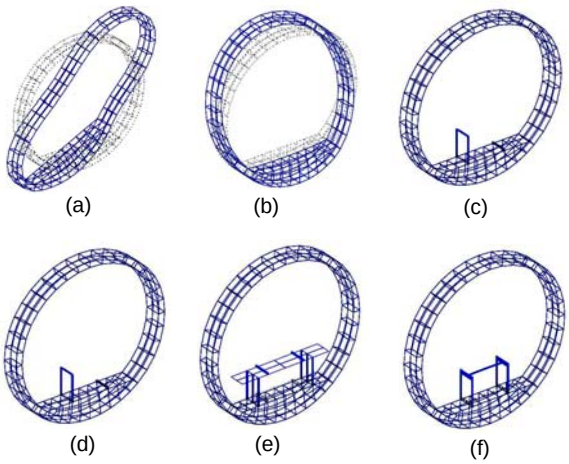

Fig. 7 Free tunnel modes and a track mode on a rigid base for each track. (a) The first in-plane free tunnel modes at 14.7 Hz; (b) The first out-of-plane free tunnel modes at 111.4 Hz; (c) The first DF mode at 186.4 Hz; (d) The first VF mode at 64.6 Hz; (e) The first FST mode at 7 Hz; (f) The first FLT mode at 35.5 Hz

Fig. 8 shows the vertical transfer functions at points A, B, C and D in the free field for different tracks. Note that the vertical axis denotes the vertical displacement Dis (dB) which can be expressed by

$$\mathrm{Dis} = 20\lg\left(\frac{D_{\mathrm{cal}}}{D_{\mathrm{ref}}}\right), \tag{18}$$

where D_{cal} is the calculated displacement, m/N, and D_{ref}=1 is the reference displacement, m/N.

3.4 Excitation loads

There are diverse excitation mechanisms $g_m(t)$ that can generate vibrations from moving trains. In general, they mainly consist of two kinds of excitation: quasi-static excitation $g_{ms}(t)$ and dynamic excitation $g_{md}(t)$ (Gupta *et al.*, 2008). The quasi-static excitation and the unevenness excitation induced by wheel and rail roughness are just considered in this study.

The quasi-static excitation is modeled as constant forces moving along the track at a train speed v. The time history $g_{ms}(t)$ is equivalent to a single axle weight w_m. The Fourier transform $\hat{g}_{ms}(\omega)$ equals $2\pi w_m\delta(\omega)$.

For the unevenness excitation, the contact force $\hat{\boldsymbol{g}}_{md}(\omega)$ (dynamic wheel-track interaction force) in the frequency domain can be calculated (Lombaert and Degrande, 2009):

$$\begin{aligned}\hat{\boldsymbol{g}}_{md}(\omega) &= [\hat{\boldsymbol{C}}^{\mathrm{v}}(\omega)+\hat{\boldsymbol{C}}^{\mathrm{tr}}(\omega)]^{-1}\hat{\boldsymbol{T}}(\omega)\sum_{i=1}^{n}\frac{-1}{\sqrt{v}}\\ &\times\sqrt{2\tilde{G}_{\mathrm{w/r}}\left(\frac{|\omega_i|}{v}\right)\Delta\omega_i}\\ &\times[\pi\delta(\omega-\omega_i)\mathrm{e}^{+j\theta_i}+\pi\delta(\omega+\omega_i)\mathrm{e}^{-j\theta_i}],\end{aligned} \tag{19}$$

where $\hat{\boldsymbol{C}}^{\mathrm{v}}(\omega)$ is the compliance of the vehicle, $\hat{\boldsymbol{C}}^{\mathrm{tr}}(\omega)$ is the compliance of the track, $\hat{\boldsymbol{T}}(\omega)$ is a vector that collects the phase shift for each axle, v is the train speed and $\tilde{G}_{\mathrm{w/r}}(|\omega_i|/v)$ is the single-sided power spectral density (PSD).

According to the Federal Railroad Administration (FRA, 2005), the track can be separated into six classes on the basis of the rail quality. The class 1 track is used to calculate the single-sided PSD $\tilde{G}_{\mathrm{w/r}}(k_y)$ in this study. The $\tilde{G}_{\mathrm{w/r}}(k_y)$ varies approximately with k_y^{-4}, therefore, the contact force $\hat{\boldsymbol{g}}_{md}(\omega)$ due to unevenness excitation approximately increases with $v^{1.5}$ from Eq. (19).

Fig. 9 shows the contact forces $\hat{\boldsymbol{g}}_{md}(\omega)$ at the front axle of the train as a function of the frequency at different speeds of 30 km/h, 45 km/h, 60 km/h and 80 km/h. For each track, the first peak exhibits at the anti-resonance frequency of the bogie mass on the primary and the second suspensions. For four tracks, the second peaks appear at around 60 Hz (DF), 26 Hz (VF), 63 Hz (FST) and 26 Hz (FLT), respectively, which are the wheel-track resonance frequencies. With the increase of train speed, the magnitude of the contact forces rises with $v^{1.5}$ for each track. Below 7 Hz, the vibration of the train plays a leading role. However, in the frequency range between 7 and 100 Hz, the interaction between the wheel and the track takes a primary role, and there exits obvious differences among the frequency content of the contact forces for four tracks, which are due to the variation of eigenfrequencies of four tracks.

3.5 Response during the passage of a train

When the transfer functions and the excitation loads in the frequency-wavenumber domain have been obtained, the response during the passage of a train can be computed by adding the contribution of the quasi-static and dynamic forces in the frequency domain from Eq. (14).

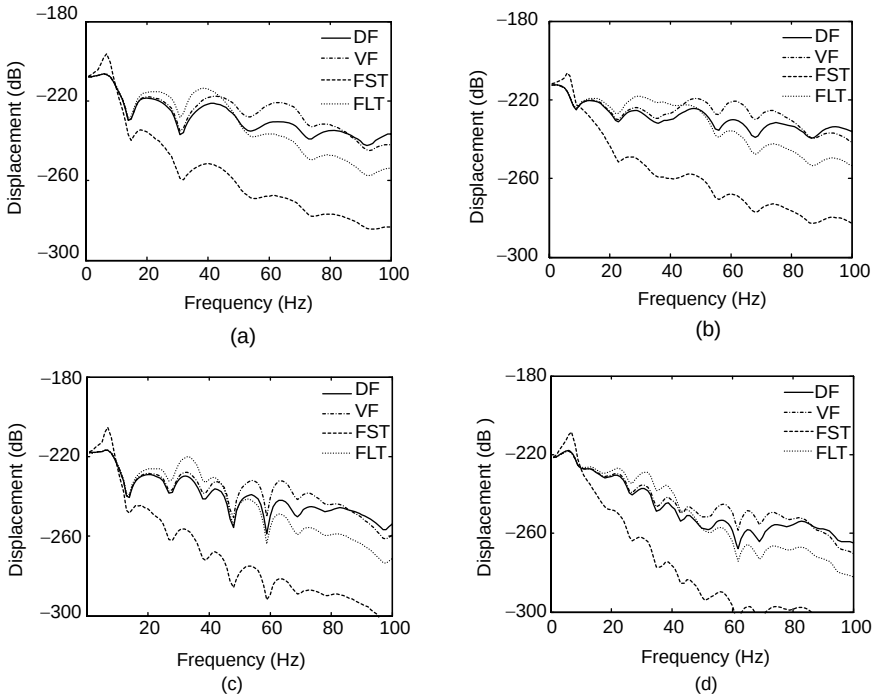

Fig. 8 Vertical transfer functions in the free field at different points. (a) A (0 m); (b) B (20 m); (c) C (40 m); (d) D (60 m)

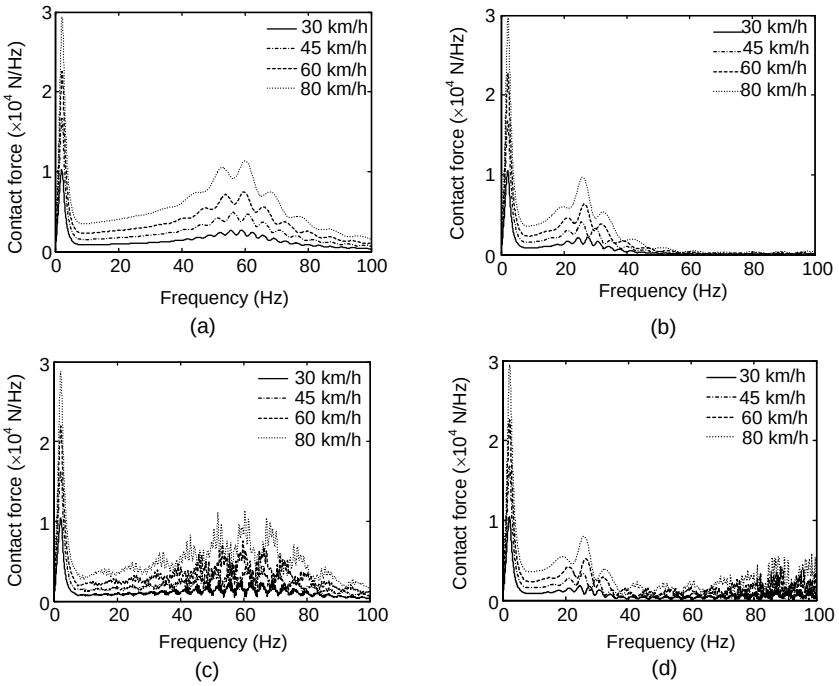

Fig. 9 Contact forces at the front axle of the train as a function of the frequency for four tracks. (a) DF; (b) VF; (c) FST; (d) FLT

Fig. 10 shows the time history and frequency content of the vertical velocity in the free field at point A at a train speed of 80 km/h. From the time history, the peak particle velocity (PPV) in the DF model is the biggest in all track models, and it is the smallest in the FST model. The PPV in the VF model is very close to that in the FLT model. For the frequency content, it is very clear that the contribution of the

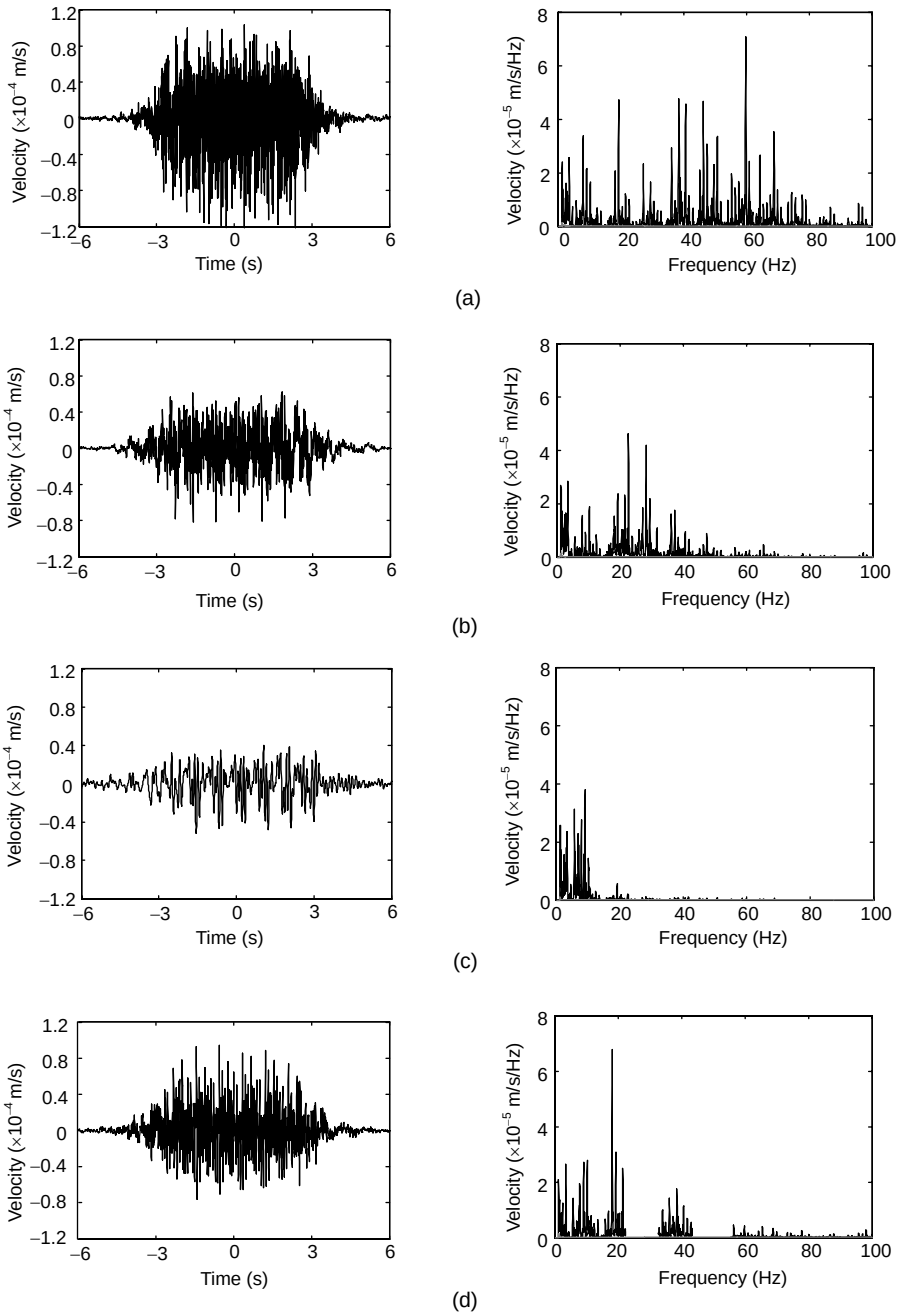

Fig. 10 Time history (left) and frequency content (right) of the vertical velocity in the free field at point A at a train speed of 80 km/h for four tracks. Superimposed on the frequency content is the contribution of quasi-static excitation (gray line). (a) DF; (b) VF; (c) FST; (d) FLT

quasi-static excitation is insignificant; however, the dynamic excitation due to the rail unevenness dominates the response in the free field. The dominant frequency content is just about the wheel-track resonance frequency for the DF, VF and FLT, however, for the FST, it is around the natural frequency of the FST.

Fig. 11 illustrates the one-third octave band root mean square (RMS) spectra of the vertical velocity in the free field at points A, B, C and D for the DF at different train speeds of 30 km/h, 45 km/h, 60 km/h and 80 km/h. The maximum allowable RMS value of the vertical velocity for the Tecnai30 electron microscope in the National Measurement Laboratory

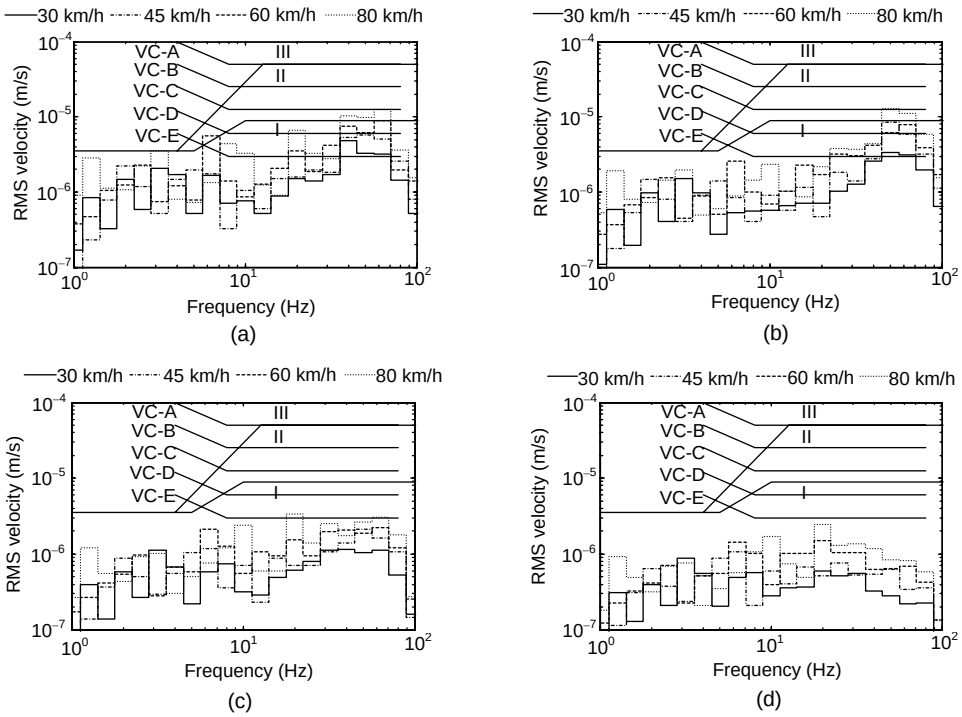

Fig. 11 One-third octave band RMS spectra of the vertical velocity for the DF at different points. (a) A (0 m); (b) B (20 m); (c) C (40 m); (d) D (60 m)

and the vibration criterion (VC) curves (Gordon, 1999) are superimposed on the graphs. If all frequency components enter zone I, the high resolution performance of the electron microscope will not be affected. If some frequency components lie in zone II, the measurement results must need to be further analyzed. If some frequency components locate in zone III, the site is unacceptable for the installation of the equipment. The VC curves are composed of five criterion curves A through E. These VC curves are merely shown as a reference order of magnitude which can help to interpret the vibration levels better.

The dependence of the one-third octave band RMS value on the train speed is identical to that of the contact force on the train speed. Thus, with the increasing speed, the velocity response at all points and all frequencies rises in the same manner as the contact forces. The amplitude of RMS value decreases with the lateral distance.

At points A and B, the RMS values of the predicted velocity at the train speed of 80 km/h enter zone II at frequencies about the wheel-track resonance frequency. The maximum RMS value of the predicted velocity is below the VC-C curve, which allows maximal level of 12.5 mm/s. At points C and D, all of the RMS values lie in zone I. At point C, the maximum RMS value of the predicted velocity is below the VC-D curve, which allows maximal level of 6 mm/s. At point D, the maximum RMS value of the predicted velocity is below the VC-E curve, which allows maximal level of 3 mm/s.

Fig. 12 gives the one-third octave band RMS spectra of the vertical velocity in the free field at points A, B, C and D for the VF at different train speeds of 30 km/h, 45 km/h, 60 km/h and 80 km/h. The dependence of the one-third octave band RMS value on the train speed is identical to that in the DF. The amplitude of RMS value also decreases with the lateral distance.

At point A, the RMS values of the predicted velocity at the train speeds of 60 km/h and 80 km/h enter zone III at frequencies below 4 Hz. The maximum RMS value of the predicted velocity is below the VC-C curve. At points B, C and D, all of the RMS values lie in zone I. At point B, the maximum RMS value of the predicted velocity is below the VC-C curve, and at points C and D, the maximum RMS value of the predicted velocity is below the VC-D curve.

Fig. 13 shows the one-third octave band RMS spectra of the vertical velocity in the free field at points A, B, C and D for the FST at different train speeds of 30 km/h, 45 km/h, 60 km/h and 80 km/h. The dependence of the one-third octave band RMS value on the train speed is also identical to that in the DF. The amplitude of RMS value goes down with the lateral distance.

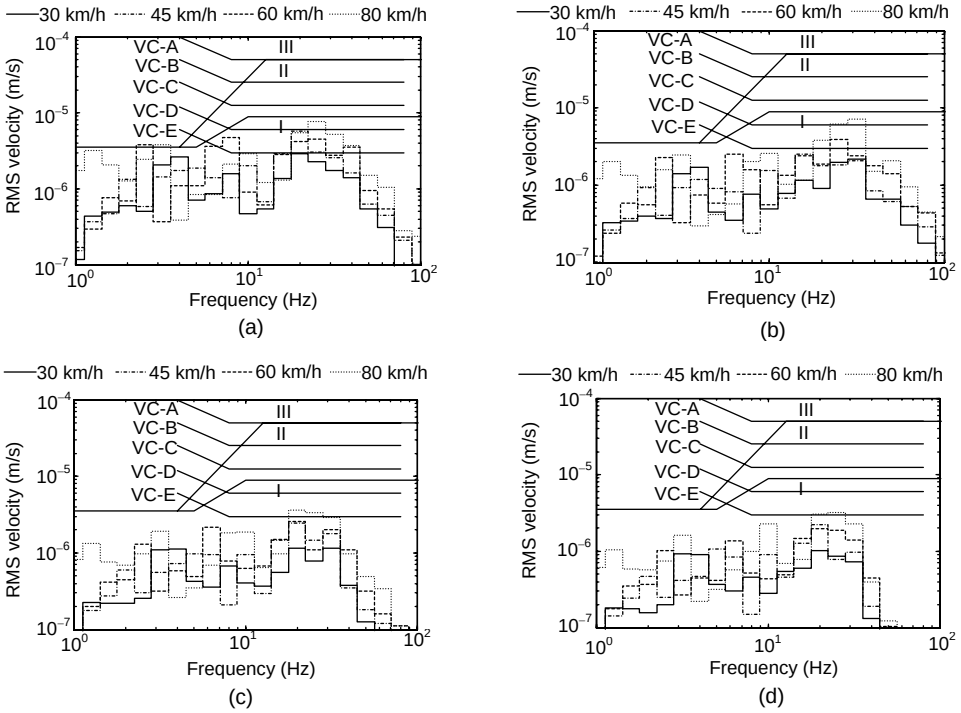

Fig. 12 One-third octave band RMS spectra of the vertical velocity for the VF at different points. (a) A (0 m); (b) B (20 m); (c) C (40 m); (d) D (60 m)

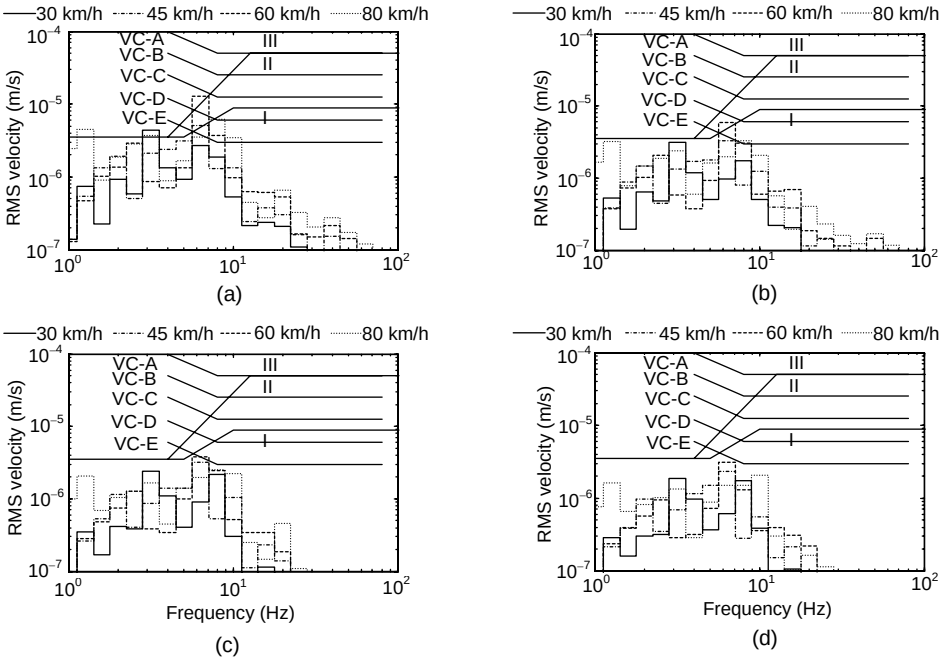

Fig. 13 One-third octave band RMS spectra of the vertical velocity for the FST at different points. (a) A (0 m); (b) B (20 m); (c) C (40 m); (d) D (60 m)

At point A, the RMS values of the predicted velocity just lie in zone III at frequencies below 7 Hz. The maximum RMS value of the predicted velocity is below the VC-C curve. At point B, the RMS values of the predicted velocity at a train speed of 60 km/h enter zone II at frequencies around 7 Hz, and the maximum RMS value of the predicted velocity is below the VC-D curve. At points C and D, all of the RMS values lie in zone I. At point C, the maximum RMS value of the predicted velocity is below the VC-D curve, and at point D, the maximum RMS value of the predicted velocity is below the VC-E curve.

Fig. 14 shows the one-third octave band RMS spectra of the vertical velocity in the free field at points A, B, C and D for the FLT at different train speeds of 30 km/h, 45 km/h, 60 km/h and 80 km/h. The dependence of the one-third octave band RMS value on the train speed is also the same to that in the DF. The amplitude of RMS value reduces with the lateral distance.

At point A, the RMS values of the predicted velocity at the train speeds of 60 km/h and 80 km/h enter zone II at frequencies around the wheel-track resonance frequency. The maximum RMS value of the predicted velocity is below the VC-C curve. At points B, C and D, all of the RMS values lie in zone I, and the maximum RMS value of the predicted velocity is below the VC-D curve.

Fig. 15 compares the vibration isolation efficiency between four tracks at a train speed of 80 km/h at points A, B, C and D. The DF, VF and FLT can attenuate vibrations well at frequencies above the wheel-track resonance frequency. The FST can attenuate vibrations well at frequencies above its natural frequency. At frequencies between 10 Hz and 100 Hz, the velocity response can be significantly reduced by means of the FST. As above-mentioned, a lot of sensitive equipments in the National Measurement Laboratory are placed in the region of 40 m far away from the tunnel centerline. Hence, they can work without interference from only metro trains induced vibrations.

4 Conclusion

A primary objective of this paper is to predict the free field vibrations due to trains on line 8 of Beijing metro, using the state-of-the-art 3D coupled periodic FE-BE method. The impact of vibrations induced by trains running on four kinds of track structures (DFs, VFs, an FST and an FLT) on sensitive equipments are compared. The following conclusions have been drawn from the above analyses:

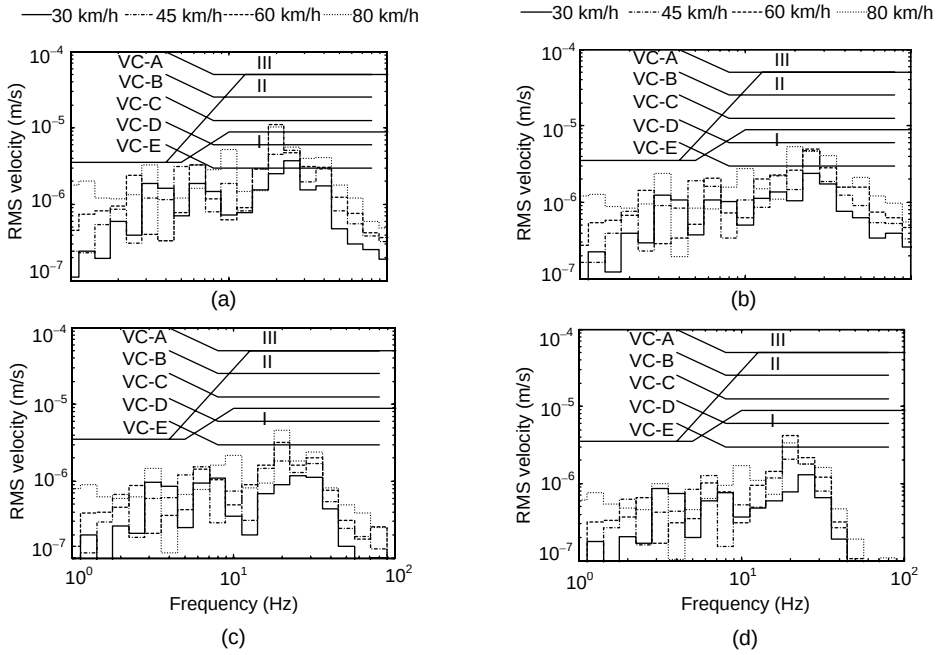

Fig. 14 One-third octave band RMS spectra of the vertical velocity for the FLT at different points. (a) A (0 m); (b) B (20 m); (c) C (40 m); (d) D (60 m)

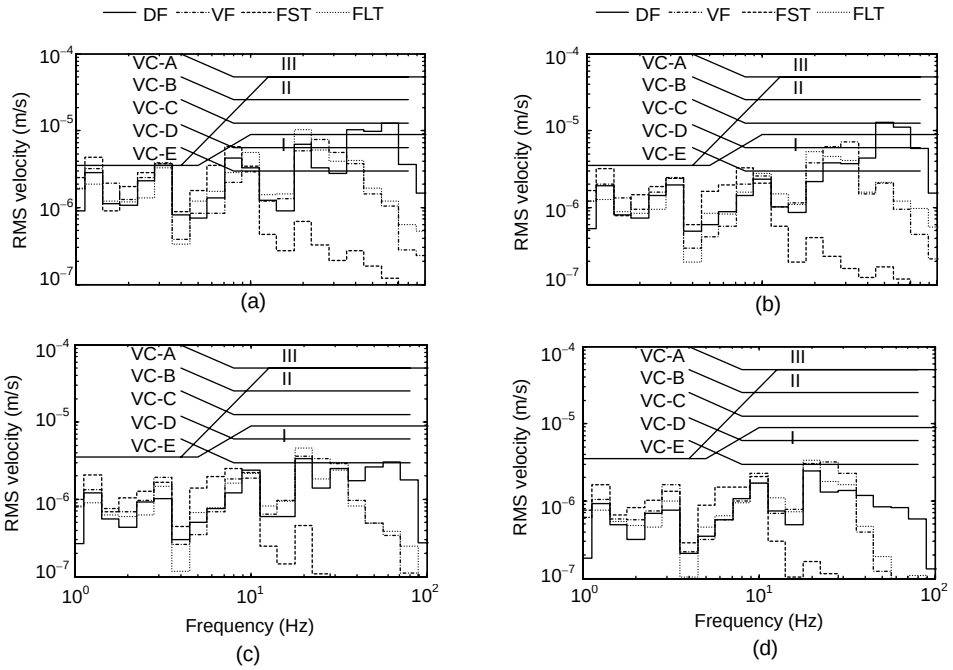

Fig. 15 One-third octave band RMS spectra of the vertical velocity at a train speed of 80 km/h at different points. (a) A (0 m); (b) B (20 m); (c) C (40 m); (d) D (60 m)

1. The natural frequencies of four tracks are about 186.4 Hz (DF), 64.6 Hz (VF), 7 Hz (FST) and 35.5 Hz (FLT), respectively.

2. The response in the free field is dominated by the dynamic excitation due to wheel and rail roughness, and the contribution of the quasi-static excitation can be negligible.

3. The response in the free field increases with the train speed v, and is approximately proportional to $v^{1.5}$. The amplitude of the response in the free field decreases with the lateral distance.

4. The comparison of the one-third octave band RMS spectra of the predicted velocity and the maximum allowable velocity for the Tecnai30 electron microscope implies that the vibrations induced only by metro trains might surpass the allowable levels at frequencies around the wheel-track resonance frequency (DF, VF and FLT) or the natural frequency (FST) at the distances below 40 m. However, when the lateral distance is larger than 40 m, the predicted values can satisfy the performance of sensitive equipments.

5. The FST with a natural frequency of 7 Hz can be very effective in attenuating vibrations. Compared with the DF, VF and FLT, the response in the free field can be more significantly reduced by means of the FST at frequencies above 10 Hz.

In terms of the vibration theory, this paper presents the applicability of the coupled periodic FE-BE method to study the efficiency of vibration isolation measures. It is necessary to calibrate and validate the FE-BE model by in situ measurements in further research work to improve the accuracy of predicted results.

References

Bampton, M.C.C., Craig, R.R.Jr., 1968. Coupling of substructures for dynamic analyses. *AIAA Journal*, **6**(7):1313-1319. [doi:10.2514/3.4741]

Chebli, H., Ramzi, O., Clouteau, D., 2006. Response of periodic structures due to moving loads. *Comptes Rendus Mécanique*, **334**(6):347-352. [doi:10.1016/j.crme.2006.04.001]

Clouteau, D., Elhabre, M.L., Aubry, D., 2000. Periodic BEM and FEM-BEM coupling: application to seismic behaviour of very long structures. *Computational Mechanics*, **25**(6):567-577. [doi:10.1007/s004660050504]

Clouteau, D., Arnst, M., Al-Hussaini, T.M., Degrande, G., 2005. Free field vibrations due to dynamic loading on a tunnel embedded in a stratified medium. *Journal of Sound and Vibration*, **283**(1-2):173-199. [doi:10.1016/j.jsv.2004.04.010]

Degrande, G., Clouteau, D., Othman, R., Arnst, M., Chebli, H., Klein, R., Chatterjee, P., Janssens, B., 2006. A numerical model for ground-borne vibrations from underground

railway traffic based on a periodic finite element-boundary element formulation. *Journal of Sound and Vibration*, **293**(3-5):645-666. [doi:10.1016/j.jsv.2005.12.023]

Ding, D.Y., Liu, W.N., Sun, X.J., Xie, D.W., 2007. Three-dimensional Numerical Study on Vibration Isolation Performance of Special Floating Slab Track. Proceedings of the 3rd International Symposium on Environmental Vibrations: Prediction, Monitoring, Mitigation and Evaluation, National Taiwan University, Taipei, p.501-508.

Ding, D.Y., Gupta, S., Lombaert, G., Liu, W.N., Degrande, G., 2008. The Prediction of Vibrations Induced by Underground Railway Traffic on Line 8 of Beijing Metro. Bilateral Project BIL/07/07, Report BWM-2008-22, K. U. Leuven, Belgium and Beijing Jiaotong University, China.

FRA (Federal Railroad Administration), 2005. High-speed Ground Transportation Noise and Vibration Impact Assessment. HMMH Report No. 293630-4, Washington, D.C.

Gordon, C.G., 1999. Generic Criteria for Vibration-sensitive Equipment. Proc. SPIE, Optomechanical Engineering and Vibration Control, **3786**:22-33. [doi:10.1117/12.363802]

Gupta, S., 2008. Numerical Modelling of Subway Induced Vibrations. PhD Thesis, Department of Civil Engineering, K. U. Leuven, Belgium.

Gupta, S., Liu, W.F., Degrande, G., Lombaert, G., Liu, W.N., 2008. Prediction of vibrations induced by underground railway traffic in Beijing. *Journal of Sound and Vibration*, **310**(3):608-630. [doi:10.1016/j.jsv.2007.07.016]

Hosking, R.J., Milinazzo, F., 2007. Floating ladder track response to a steadily moving load. *Mathematical Methods in the Applied Sciences*, **30**(14):1823-1841. [doi:10.1002/mma.871]

Kuo, C.M., Huang, C.H., Chen, Y.Y., 2008. Vibration characteristics of floating slab track. *Journal of Sound and Vibration*, **317**(3-5):1017-1034. [doi:10.1016/j.jsv.2008.03.051]

Liu, W.F., Gupta, S., Degrande, G., Liu, W.N., 2006. Numerical Modelling of Vibrations Induced by Underground Railway Traffic on Metro Line 4 in Beijing. Bilateral Project BIL/04/17, Report BWM-2006-08, K. U. Leuven, Belgium.

Liu, W.N., Ding, D.Y., Sun, X.J., Liu, W.F., 2005. Study on Special Vibration Reduction Measures in Beijing Metro Line 4. Report 2005-08, Beijing Jiaotong University, Beijing, China (in Chinese).

Lombaert, G., Degrande, G., 2009. Ground-borne vibration due to static and dynamic axle loads of InterCity and high-speed trains. *Journal of Sound and Vibration*, **319**(3-5):1036-1066. [doi:10.1016/j.jsv.2008.07.003]

Lombaert, G., Degrande, G., Vanhauwere, B., Vandeborght, B., François, S., 2006. The control of ground-borne vibrations from railway traffic by means of continuous floating slabs. *Journal of Sound and Vibration*, **297**(3-5):946-961. [doi:10.1016/j.jsv.2006.05.013]

Nelson, J.T., 1996. Recent developments in ground-borne noise and vibration control. *Journal of Sound and Vibration*, **193**(1):367-376. [doi:10.1006/jsvi.1996.0277]

Okuda, H., Asanuma, K., Matsumoto, N., Wakui, H., 2004. Dynamic load, resistance and environmental performance of floating ladder track. *Quarterly Report of RTRI*, **45**(3):149-155. [doi:10.2219/rtriqr.45.149]

Wilson, G.P., Saurenman, H.J., Nelson, J.T., 1983. Control of ground-borne noise and vibration. *Journal of Sound and Vibration*, **87**(2):339-350. [doi:10.1016/0022-460X(83)90573-4]

Xia, H., Deng, Y.S., Zou, Y.W., de Roeck, G., Degrande, G., 2009. Dynamic analysis of rail transit elevated bridge with ladder track. *Frontiers of Architecture and Civil Engineering in China*, **3**(1):2-8. [doi:10.1007/s11709-009-0001-x]